A&A 524, A55 (2010)
DOI: 10.1051/0004-6361/201015132

Astronomy & Astrophysics

Transiting exoplanets from the *CoRoT* space mission

XIV. CoRoT-11b: a transiting massive "hot-Jupiter" in a prograde orbit around a rapidly rotating F-type star⋆

D. Gandolfi[1,2], G. Hébrard[3], R. Alonso[4], M. Deleuil[5], E. W. Guenther[1], M. Fridlund[2], M. Endl[6], P. Eigmüller[1], Sz. Csizmadia[7], M. Havel[8], S. Aigrain[9], M. Auvergne[10], A. Baglin[10], P. Barge[5], A. S. Bonomo[5], P. Bordé[11], F. Bouchy[3,12], H. Bruntt[10], J. Cabrera[7,13], S. Carpano[2], L. Carone[14], W. D. Cochran[6], H. J. Deeg[15], R. Dvorak[16], J. Eislöffel[1], A. Erikson[7], S. Ferraz-Mello[17], J.-C. Gazzano[5,8], N. B. Gibson[9], M. Gillon[4,18], P. Gondoin[2], T. Guillot[8], M. Hartmann[1], A. Hatzes[1], L. Jorda[5], P. Kabath[7,19], A. Léger[11], A. Llebaria[5], H. Lammer[20], P. J. MacQueen[6], M. Mayor[4], T. Mazeh[21], C. Moutou[5], M. Ollivier[11], M. Pätzold[14], F. Pepe[4], D. Queloz[4], H. Rauer[7,22], D. Rouan[10], B. Samuel[11], J. Schneider[13], B. Stecklum[1], B. Tingley[15], S. Udry[4], and G. Wuchterl[1]

(Affiliations can be found after the references)

Received 2 June 2010 / Accepted 30 August 2010

ABSTRACT

The *CoRoT* exoplanet science team announces the discovery of CoRoT-11b, a fairly massive hot-Jupiter transiting a $V = 12.9$ mag F6 dwarf star ($M_* = 1.27 \pm 0.05\ M_\odot$, $R_* = 1.37 \pm 0.03\ R_\odot$, $T_{\rm eff} = 6440 \pm 120$ K), with an orbital period of $P = 2.994329 \pm 0.000011$ days and semi-major axis $a = 0.0436 \pm 0.005$ AU. The detection of part of the radial velocity anomaly caused by the Rossiter-McLaughlin effect shows that the transit-like events detected by *CoRoT* are caused by a planet-sized transiting object in a prograde orbit. The relatively high projected rotational velocity of the star ($v \sin i_\star = 40 \pm 5$ km s^{-1}) places CoRoT-11 among the most rapidly rotating planet host stars discovered so far. With a planetary mass of $M_{\rm p} = 2.33 \pm 0.34\ M_{\rm Jup}$ and radius $R_{\rm p} = 1.43 \pm 0.03\ R_{\rm Jup}$, the resulting mean density of CoRoT-11b ($\rho_{\rm p} = 0.99 \pm 0.15$ g/cm^3) can be explained with a model for an inflated hydrogen-planet with a solar composition and a high level of energy dissipation in its interior.

Key words. planetary systems – techniques: photometric – techniques: radial velocities – techniques: spectroscopic

1. Introduction

Discovering and studying extrasolar planets, and in general planetary systems other than ours, aims at understanding whether the solar system is peculiar and unique or usual and unremarkable. In this context, the discovery of a large population of Jupiter-like planets with a semi-major axis $\lesssim$0.1 AU (i.e., hot-Jupiters), as well as the detection of massive planets in very eccentric orbits (Moutou et al. 2009a; O'Toole et al. 2009) or even strongly misaligned with the stellar spin axis (Hébrard et al. 2008; Pont et al. 2009), has proven how the properties of extrasolar planets can be surprisingly different from those observed in the solar system's planets.

From this point of view, studies of transiting extrasolar planets are cornerstones for understanding the nature of planets beyond the solar system, since a wealth of precious information can be gained (Winn 2010). Indeed, the peculiar geometry of transiting planets makes them very special targets for obtaining direct measurements of the planet-to-star radius (e.g., Rosenblatt 1971; Borucki & Summers 1984). By combining time-series photometric observations acquired during the transit with radial velocity (RV) measurements of the host star, it is possible to derive the radius and mass of the planet, and therefore its mean density, once the mass and radius of the star has been determined. Transits also offer a unique opportunity to measure the sky-projected angle (λ) between the orbital angular momentum vector and the spin axis of the star (Gaudi & Winn 2007). This can be done by detecting the Rossiter-McLaughlin (RM) effect, i.e., the spectral distortion observed in the line profile of a rotating star as a second object passes in front of the stellar disc.

Furthermore transit surveys have the potential to enlarge the parameter space of planet host stars by detecting planets around stars that are usually not observed in radial velocity surveys. As is well known, Doppler surveys typically focus on slowly rotating solar-like stars because high RV precision can easily be achieved. They usually discard more massive main-sequence stars for which accurate RV measurements are rendered unfeasible by the rapid stellar rotation rate and the paucity of spectral lines. Indeed, a few RV searches have been conducted up to now around A- and F-type stars (e.g., Lagrange et al. 2009; Guenther et al. 2009; Bowler et al. 2010; Johnson et al. 2010). Transit detections are not affected by the stellar rotation and can lead to the discovery of planets around rapidly rotating stars.

Space missions like *CoRoT* (Co*nvection*, Ro*tation, and planetary* T*ransits*, Baglin et al. 2006; Auvergne et al. 2009) and *Kepler* (Borucki et al. 2010; Koch et al. 2010) are crucial to increase the number of planets with well-known orbital and physical parameters, and consequently improve the database that is needed to investigate all the aspects of the exoplanets population, down to the Earth-like mass-regime. The recent discoveries announced by the *CoRoT* exoplanet science team fully demonstrate the capability of the mission to populate the mass-radius

⋆ The *CoRoT* space mission, launched on 2006 December 27, has been developed and is operated by CNES, with the contribution of Austria, Belgium, Brazil, ESA (RSSD and Science Programme), Germany and Spain.

diagram, from the "transition desert regime" between brown dwarfs and planets (Deleuil et al. 2008), across hot and temperate Jupiter-like objects (Barge et al. 2008; Alonso et al. 2008; Bouchy et al. 2008; Aigrain et al. 2008; Moutou et al. 2008; Rauer et al. 2009; Fridlund et al. 2010; Deeg et al. 2010), and down to the Earth-like radius regime (Léger et al. 2009; Queloz et al. 2009).

In the present paper the *CoRoT Exoplanet Science Team* announces its eleventh transiting planet, namely CoRoT-11b, a fairly massive Jupiter-like planet in a relatively short-period orbit (about three days) around a rapidly rotating F6 dwarf star. By combining the high-precision photometric data from *CoRoT* with RV measurements and high signal-to-noise spectroscopy from the ground, we fully characterised the planet's orbit and derived the main physical parameters of the planet-star system. Thanks to time-series RV measurements acquired during the transit we observed part of the RM effect and confirm the planetary transit event.

2. *CoRoT* observations, data reduction, and analysis

2.1. Satellite observations

CoRoT-11b was discovered during the *CoRoT*'s second long run towards the Galactic centre direction, i.e., the *CoRoT LRc02* run[1]. The observations lasted 145 days, from 2008 April 15 to September 7. The *LRc02* field is centred at $\alpha \approx 18^{\rm h}42^{\rm m}$ and $\delta \approx 6°39'$ (J2000), between the *Ophiuchus* and the *Serpens Cauda* constellations. The planet was detected transiting the *CoRoT* star[2] with ID=0105833549. The main designations of the planet host star CoRoT-11 along with its equatorial coordinates and optical and near-infrared photometry, are reported in Table 1 as retrieved from the *ExoDat* database (Deleuil et al. 2009) and *2MASS* catalogue (Cutri et al. 2003).

The transiting planet was detected after 51 days of observations in the so-called *CoRoT alarm-mode* (Quentin et al. 2006; Surace et al. 2008). This observing strategy consists in processing and analysing a first set of photometric data in order to single out planetary transits while the *CoRoT* run is still on-going. This enabled us to switch the time sampling of the light curve from 512 to 32 s and trigger the ground-based follow-up observations (see Sect. 3). Thanks to an objective prism in the optical path of the *CoRoT* exoplanet channel (Auvergne et al. 2009), CoRoT-11 was observed in three broad-band colours (red, green, and blue), according to the specific photometric mask selected at the beginning of the run. This usually allows us to remove false positives that mimick planetary transit events, such as stellar activity or eclipsing binaries. A total of 261 917 photometric data-points were collected for each colour channel, 8349 of those were obtained with a time sampling of 512 s, and 253 568 with 32 s. The transit signal was detected in all three colour channels with the similar depth and the same duration and ephemeris as expected for a *bona-fide* planetary transit.

At the end of the *LRc02* observing run, the whole photometric data-set of CoRoT-11 was processed using the *CoRoT* reduction and calibration package described in Auvergne et al. (2009). The pipeline also flags bad photometric data-points collected during the entrance into and exit from the Earth's shadow or data-points that are strongly affected by hits of high-energy particles resulting from the crossing of the south atlantic anomaly (SAA).

[1] The "*LR*" prefix means that the field is a long-run field (typically 150 days of observations). The letter "*c*" refers to the Galactic centre direction. The last two digits "*02*" indicate that the observed field is the second *CoRoT* long-run towards the Galaxy centre.

[2] See Carpano et al. (2009) for a full description of the *CoRoT* target nomenclature.

Table 1. CoRoT, GSC2.3, USNO-A2, and 2MASS identifiers of the planet host star CoRoT-11.

Main identifiers		
CoRoT ID	0105833549	
GSC2.3 ID	N1RO000587	
USNO-A2 ID	0900-13499974	
2MASS ID	18424494+0556156	
Coordinates		
RA (J2000)	$18^{\rm h}42^{\rm m}44\overset{\rm s}{.}95$	
Dec (J2000)	$05°\ 56'\ 16\overset{''}{.}12$	
Magnitudes		
Filter	Mag	Error
B	13.596	0.024
V	12.939	0.019
r'	12.638	0.019
i'	12.283	0.053
J	11.589	0.021
H	11.416	0.029
*K*s	11.248	0.022

Notes. Equatorial coordinates, optical, and near infrared photometry are from the *ExoDat* catalogue (Deleuil et al. 2009) and *2MASS* catalogue (Cutri et al. 2003).

2.2. CoRoT light curve and transit fit

In order to increase the signal-to-noise (S/N) ratio, the analysis of the photometric data was performed using the white light curve, as derived by adding together the signal from the three colour channels. CoRoT-11 has a close neighbour star at about 2″ northwest, falling well inside the *CoRoT* photometric aperture, as well as a handful of faint nearby stars that are spatially located around the *CoRoT* mask (see also Sect. 3.1 and Fig. 3). According to the *ExoDat* database, the closest neighbour star is 2.1 mag fainter than CoRoT-11 in the *r'*-band. Following the method described in previous *CoRoT* papers (e.g., Alonso et al. 2008), we estimated that it contributes about 12.2% of the total flux of the photometric mask of CoRoT-11. Taking also into account the light coming from the fainter neighbours, the total contamination fraction rises up to $13.0 \pm 1.5\%$. This fraction was removed from the whole data-set prior to analysing the white light curve.

A first cleaning of the raw *CoRoT* data was performed applying an iterative sigma-clipping algorithm. Most of the photometric points rejected according to this criterion (about 7.8%) resulted from the crossing of the SAA and matched the photometric data previously flagged as outlier by the *CoRoT* automatic pipeline (Auvergne et al. 2009). The cleaned white light curve is plotted in Fig. 1. It shows 49 transits with a depth of ∼1.1%, occurring about every three days. The transits are clearly visible, as shown in the inset of Fig. 1. Out of 49 transits, 17 were detected with a 512 s time sampling, whereas 32 were observed with the oversampled rate (32 s). The light curve is moderately affected by sudden "jumps" in intensity resulting from the impact of high-energy particles onto the *CoRoT* CCDs (Pinheiro da Silva et al. 2008). The high-frequency scatter of the

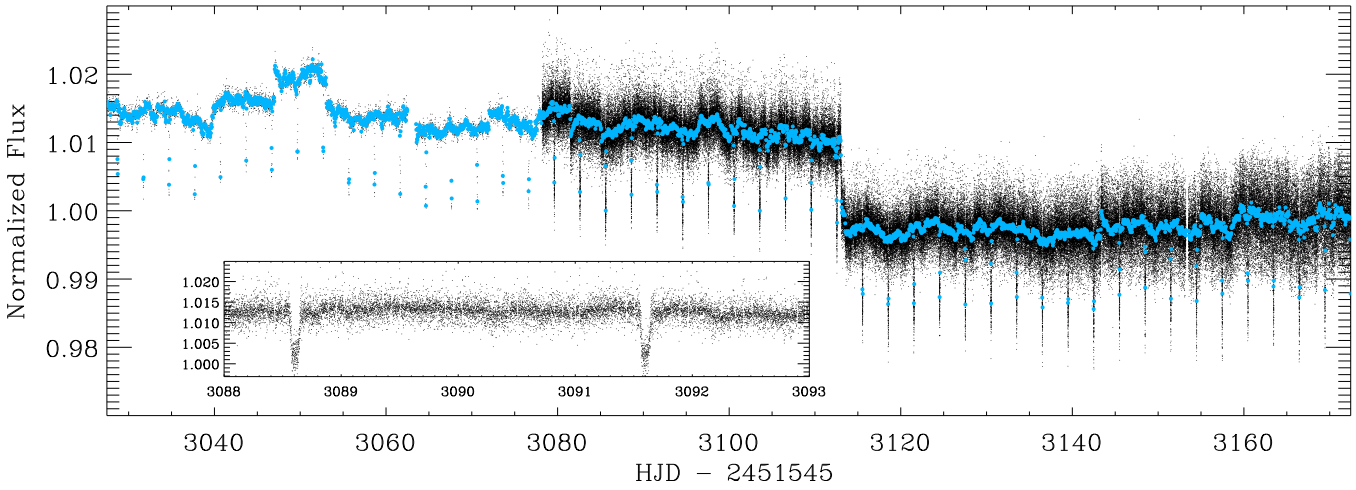

Fig. 1. Whole (145 days) cleaned light curve of CoRoT-11, sampled at 512 s from the first ~50 days, and at 32 s until the end of the run. For the sake of clarity, the blue dots represent 1-h binned points. The inset plot is a zoom of the light curve showing two transits of CoRoT-11b. The "jumps" observed in the plot are caused by the impacts of high-energy particles onto the CCD's lattice. The light curve has been arbitrarily normalised to the median value of the flux. See the online edition of the Journal for a colour version of this figure.

light curve (Fig. 1) is compatible with other sources of similar brightness observed by *CoRoT* Aigrain et al. (2009).

The *CoRoT* light curves are affected by a modulation of the satellite orbital period, which changes its shape and amplitude during a long run observation. Following the prescription of Alonso et al. (2008), the orbital signal of each *j*th orbit was corrected with the signals from the previous and the following 30 orbits. The data points acquired during the transits were not considered in the estimate of the mean orbital signal of the *j*th orbit.

In order to determine the period P and transit epoch $T_{\rm tr}$, we first used an approximate ephemeris to build a phase-folded curve of the transit. A simple trapezoidal model was fitted to this curve to get the parameters of the average transit, i.e., depth, duration, centre, and ingress/egress time. This model was then fitted to each individual transit, leaving only the centre as free parameter. A linear fit to the final observed-calculated (O–C) diagram of the transit centres served to refine the ephemeris, and we iterated the process until the fitted line had no significant slope. Once the orbital period and transit epoch were derived (Table 4), we constructed a combined phase-folded transit curve to this ephemeris by successively normalising each transit to the regions surrounding it. In this case, because the star is not very active (see Fig. 1), we used simple line fits to the phases between $[-0.06, -0.02]$, and $[0.02, 0.06]$, using the ephemeris of Table 4, and applied this normalisation to the whole section from phases $[-0.06, 0.06]$. We used a Savitzky-Golay filter to recognize a few remaining outliers before binning in phase. Taking into account the photometry rejected according to the first sigma-clipping algorithm, this process removed about 1.6% of the remaining data points, leading to a final duty cycle of ~90%.

Finally, the data-points were binned in blocks of 0.0005 in phase, and the error bars were estimated as the standard deviation of the data points inside each bin divided by the square root of the number of points inside the bin. The phase-folded curve of the transit is shown in Fig. 2.

The transit was fitted to a model using the formalism of Giménez (2006). To find the solution that best matches our data, we minimized the χ^2 using the algorithm AMOEBA (Press et al. 1992). The fitted parameters were the centre of the transit, the phase of start of the transit θ_1, the planet-to-star radius ratio

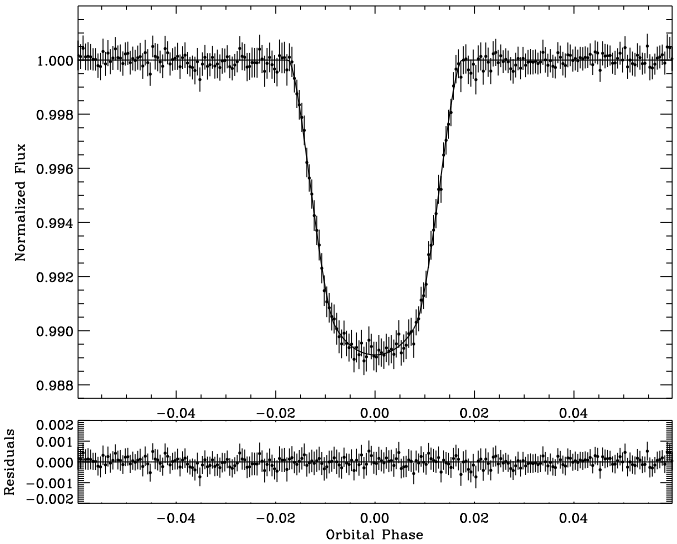

Fig. 2. Binned and phase-folded curve of the transit of CoRoT-11b, with the best-fit model over-plotted and the residuals of the fit. The standard deviation of the points outside transit is of 230 ppm (with a phase sampling of 5×10^{-4}, corresponding to about 129 s). The mean error bar of the bins is of 239 ppm, revealing an insignificant amount of red noise in the phase-folded light curve after the corrections described in the text have been performed.

$k = R_{\rm p}/R_*$, the orbital inclination i and the two non-linear limb darkening coefficients $u_+ = u_a + u_b$ and $u_- = u_a - u_b$. We used a quadratic law for the limb darkening, given by $I(\mu) = I(1)[1 - u_a(1-\mu) - u_b(1-\mu)^2]$, where I is the distribution of brightness over the star and μ is the cosine of the angle between the normal to the local stellar surface and the line of sight. The use of u_+ and u_- is a better choice to avoid correlations between the two limb darkening coefficients u_a and u_b, as described in Giménez (2006). To estimate the errors in each of the parameters we performed the χ^2 minimization to five hundred different sets of data. These data-sets were constructed with different values for the contamination factor (estimated at 13.0 ± 1.5%), and different starting values to the AMOEBA minimization. To build each set, we first subtracted the best solution to the data,

and then circularly shifted the residuals by a random quantity to keep the low-frequency content of the noise. The best-fit solution was finally added to these new residuals. For each of the fitted parameters in all data-sets, we calculated the standard deviation as an estimate of the errors. In order to take into account the effect of the non-Gaussian distributions of the parameters, we also forced a Gaussian fit to the measured distributions. The adopted (conservatively larger) error bar was the biggest error among the standard deviation of the fitted parameters and the σ of the fitted Gaussian distribution. The parameters and associated errors are listed in Table 4, along with the scaled semi-major axis a/R_*, as derived using Eq. (12) in Giménez (2006). Assuming a circular orbit (i.e., $e = 0$) and combining the scaled semi-major axis a/R_* with the orbital period P via the Kepler's laws, we derived the parameter $M_*^{1/3}/R_* = 0.787 \pm 0.010$ in solar units, which leads to a mean stellar density $\rho_* = 0.62 \pm 0.02$ g/cm^3 (see Seager & Mallén-Ornelas 2003; Winn 2010, for the relevant formulas). The transit fit yielded the limb darkening coefficients $u_+ = 0.61 \pm 0.06$ and $u_- = 0.02 \pm 0.04$ (Table 4), in very good agreement with the theoretical values $u_+ = 0.64 \pm 0.01$ and $u_- = 0.06 \pm 0.01$ predicted by Sing (2010) for a star with the same fundamental parameters as CoRoT-11 (Sect. 3.4).

Note that the standard deviation of the residuals outside the transit phase is 230 ppm, which is within the uncertainties identical to the mean error bar of each of the bins (239 ppm), thus revealing the small low-frequency noise in the phase-folded light curve after the analysis described above.

2.3. Planetary eclipse upper limits

We searched for the eclipse of the planet in the *CoRoT* light curve with the same techniques as described in Alonso et al. (2009a,b) and Fridlund et al. (2010). To account for a possible eccentric orbit, we mapped the χ^2 levels of a fit to a trapezoid (with the shape parameters estimated from the transit) for different orbital phases. We did not obtain any significant detection above 100 ppm in depth. We can thus set an upper 3σ limit for the planetary eclipse depth of 100 ppm, which we translated into an upper limit to the brightness temperature of 2650 K (Alonso et al. 2009b).

3. Ground-based observations, data reduction, and analysis

As already described in previous *CoRoT* discovery papers, intensive ground-based observations are mandatory to establish the planetary nature of the transiting candidates detected by *CoRoT*. These follow-ups are crucial to rule out possible false positives, i.e., physical configurations that mimick planetary transits, which cannot be excluded on the basis of meticulous light curve analyses only. Out of about 50 promising candidates detected per *CoRoT* long run field (see Carpano et al. 2009; Moutou et al. 2009b; Cabrera et al. 2009; Carone et al. 2010), usually only a handful turns out to be *bona fide* planetary objects. Furthermore, ground-based observations are needed to assess the planetary nature of the transiting object, derive the true mass of the planet, and measure the stellar parameters of the host star needed to accurately compute the planet radius[3].

Follow-up campaigns of the planetary transit candidates detected by the *alarm-mode* in the *LRc02* field started in early Summer 2008. In the following subsection we will describe the complementary photometric and spectroscopic ground-based observations of CoRoT-11.

[3] We remind the reader that transits provide the direct measurement of only the planet-to-star radius ratio.

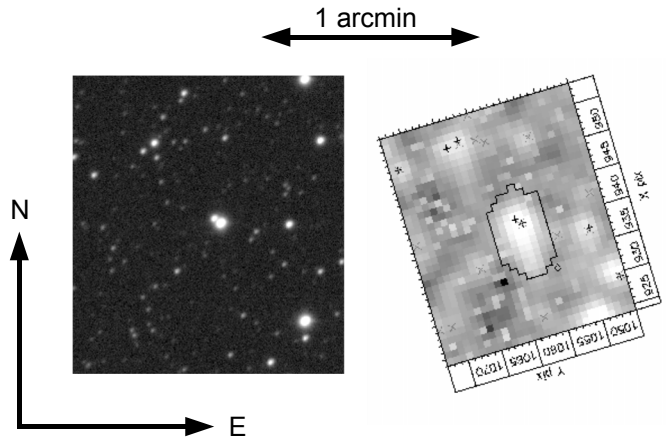

Fig. 3. Sky area around CoRoT-11. *Left*: r'-filter image as retrieved from the *ExoDat* database. CoRoT-11 is the brightest source in the centre of the image. The nearby contaminant star, about 2″ northwest from the main target, is clearly visible. *Right*: image acquired by *CoRoT*, at the same scale and orientation. The thick line around the target delimits the photometric mask used to integrate the signal of CoRoT-11. Note how the target and the contaminant are completely blurred and blended. The crosses in the image mark the position of the stars in the field.

3.1. Photometric follow-ups

The objective prism placed along the optical path of the *CoRoT* exoplanet channel spreads the light of the observed targets over about 50 pixels on the CCDs, corresponding to a projected sky area of about 20″ × 10″. The total flux of each *CoRoT* target is then computed by integrating the pixel signal over a preselected photometric mask elongated along the dispersion direction and covering most of the point spread function (PSF). As already described in Sect. 2.2, this increases the possibility that the light of neighbour stars could contaminate the flux of the *CoRoT* target. Furthermore, what is believed to be a "good" planetary transit might actually turn out to be the eclipse of a faint nearby binary system, whose light is diluted by the *CoRoT* target star.

To reproduce the observed ∼1.1% deep transit, a generic contaminant star cannot be more than ∼5 mag fainter than CoRoT-11. As already mentioned above, CoRoT-11 has a close, 2.1 mag fainter neighbour star that might thus actually be the *potential* source of false alarm (Fig. 3). In order to exclude this scenario, we took advantage of the *CoRoT* ephemeris to perform the so-called "on-off" photometry. In this procedure, candidates are photometrically observed with ground-based facilities at higher spatial resolution than *CoRoT* during the transit (on-observation) and out of the transit (off-observation). The brightness of the candidates, as well as that of any nearby stars, is then monitored to unveil any potential background eclipsing binary. Full details of this method are described in Deeg et al. (2009).

According to this observing strategy, *R*-band photometry was carried out on 2008 July 4, using the CCD camera mounted on the Swiss Leonard Euler 1.2 m telescope at La Silla Observatory (Chile), under photometric sky condition. Four sets of five consecutive exposures of 45 s each were acquired. The first set was obtained during the predicted transit

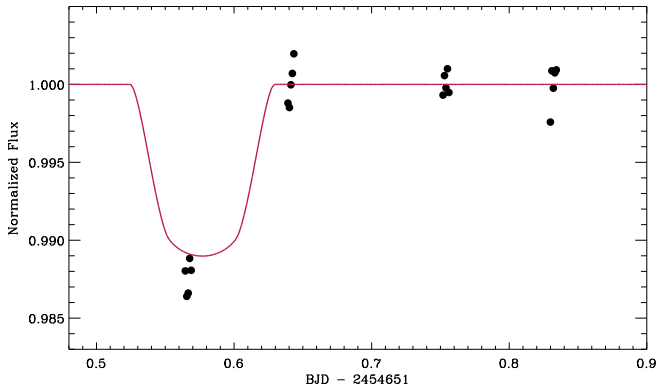

Fig. 4. *r*-band light curve of CoRoT-11 as seen with the CCD camera mounted on the Swiss Leonard Euler 1.2 m telescope at La Silla Observatory (Chile). The black circles mark each single exposure. The transit fit is over-plotted as derived from the *CoRoT* light curve analysis.

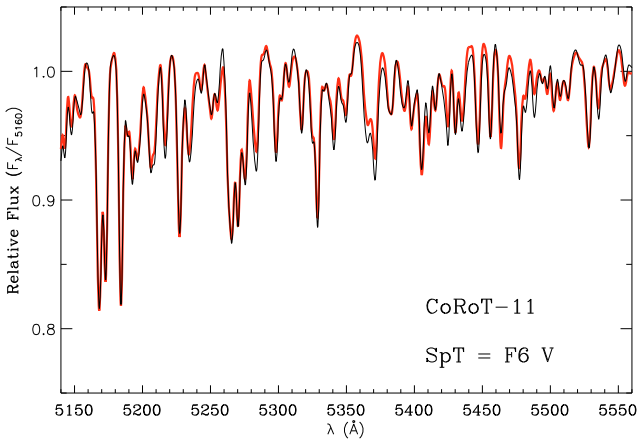

Fig. 5. Section of the TLS low-resolution spectrum of CoRoT-11 (thin black line). Overplotted with a thick red line is the best-fitting F6 V template. The spectra have been arbitrarily normalised to the flux at 5160 Å. See the online edition of the Journal for a colour version of this figure.

(on-observation), whereas the remaining three were taken out of transit (off-observations). The data were reduced with standard IRAF routines[4]; aperture photometry was performed with the DAOPHOT package under the IRAF environment. Differential photometry was obtained for CoRoT-11, as well as for the nearby contaminants, using a set of nearby comparison stars. The on-off Euler observations clearly show that CoRoT-11 is the source of the transit events detected by *CoRoT* (Fig. 4). The first photometric data-set shows a dimming of the light of CoRoT-11 at the expected time and with roughly the same depth at mid-transit. The 2.1 mag fainter star located at about 2″ north-west of the target should undergo eclipses with depths of about 0.1 mag, something which the ground-photometry clearly excluded. By centring and co-adding the best-seeing Euler images, we excluded the presence of a third nearby object down to $R \approx 17.5$ mag and up to 1.5″ from CoRoT-11.

More Johnson *R*-band photometric observations of CoRoT-11 were carried out using the 30 cm TEST telescope at the Thüringer Landessternwarte (TLS), Tautenburg (Germany), on 2008 September 7. Full details of the instrument, observing strategy, and data reduction can be found in Eislöffel et al. (2007) and Eigmüller & Eislöffel (2009). Although these observations were performed at higher time-sampling than those at Euler, they were affected by poor weather conditions, especially in the second half of the night. Nevertheless, we succeeded to observe the transit ingress of CoRoT-11b at the expected *CoRoT* ephemeris and exclude significant photometric variations in the nearby contaminant stars.

3.2. Reconnaissance low-resolution spectroscopy

Low-resolution reconnaissance spectroscopy of the planet host star was performed with the long-slit spectrograph mounted at the Nasmyth focus of the 2 m Alfred Jensch telescope of the TLS observatory, Tautenburg, Germany. These observations were part of an intensive programme devoted to the spectroscopic "snapshot" of the planetary candidates detected by the *alarm-mode* in the *LRc02 CoRoT* field. They were useful to quickly classify the stars and derive a first estimate of their photospheric parameters. Furthermore, they allowed us to identify and remove giant stars, for which the transiting object would result in a low-mass stellar companion, as well as B-type objects and rapidly rotating early-type stars, for which high-precision radial velocity measurements cannot be achieved.

CoRoT-11 was observed on 2008 August 8, under clear and stable weather conditions. Three consecutive exposures of 20 min each were acquired and subsequently combined to remove cosmic ray hits and improve the S/N ratio. The data reduction was performed with a semi-automatic pipeline developed under the IDL[5] environment. Relative flux calibration was performed observing two spectro-photometric standard stars. The final extracted and co-added spectrum covers the wavelength range 4950–7320 Å, with a resolving power $R \approx 2100$ and an average $S/N \approx 60$. The spectral type and the luminosity class of CoRoT-11 was derived by fitting the observed spectrum with a grid of suitable template spectra, as described in Frasca et al. (2003) and Gandolfi et al. (2008) and shown in Fig. 5. We found that CoRoT-11 is an F6 V star, with an accuracy of about ±1 sub-class (Table 4).

3.3. Radial velocity observations

The RV follow-up of the host star CoRoT-11 was started in summer 2008 by acquiring two high-resolution spectra with the SOPHIE spectrograph (Bouchy et al. 2009) attached to the 1.93 m telescope of the Haute-Provence Observatory (France). The instrument was set in its high efficiency (HE), leading to a resolving power of $R \approx 40\,000$. These observations revealed a rapidly rotating star with relatively broad spectral lines, corresponding to a projected rotational velocity ($v \sin i_\star$) of ~40 km s^{-1}. According to the *CoRoT* ephemeris, the SOPHIE spectra were secured around the extreme orbital phases (i.e., phase 0.25 and 0.75), and showed a RV variation of ~450 m/s in phase with the *CoRoT* ephemeris. Because the F6 V spectral type of the host star translates into a stellar mass of about 1.3 $M_\odot$, the measured RV variation is compatible with a ~2 $M_{\rm Jup}$ Jupiter planet. Twelve additional RV measurements were obtained in summer 2008 and 2009 using the HARPS spectrograph (Mayor et al. 2003) mounted at the 3.6 m ESO telescope on La Silla

[4] IRAF is distributed by the National Optical Astronomy Observatory, which is operated by the Association of Universities for Research in Astronomy (AURA), inc., under cooperative agreement with the National Science Foundation.

[5] IDL is distributed by ITT Visual Information Solutions, Boulder, Colorado.

(Chile). The spectra were acquired at different orbital phases, under good weather conditions and without strong moonlight contamination. The data were acquired setting the spectrograph both in the EGGS and HARPS standard modes, yielding a resolving power of $R \approx 70\,000$ and $R \approx 115\,000$, respectively.

The extraction of both the SOPHIE and HARPS spectra was performed using the respective pipelines. Following the techniques described by Baranne at al. (1996) and Pepe at al. (2002), the radial velocities were measured from a weighted cross-correlation of the spectra with a numerical mask. We used a standard G2 mask that includes more than 3500 lines. Cross-correlations with F0 and K5 masks gave similar results. One SOPHIE spectrum and three HARPS spectra were corrected for small moonlight contamination following the method described in Pollacco et al. (2008) and Hébrard et al. (2008), which uses a reference background sky spectrum obtained through a second fiber spatially located near the target. This led to a radial velocity correction of 700 ± 80 m/s and below 450 ± 50 m/s for the SOPHIE and HARPS spectra, respectively.

Two complementary RV measurements were acquired using the echelle spectrograph mounted on the 2 m Alfred Jensch telescope of the TLS observatory, Tautenburg (Germany), in July and August 2009. For each observing night, two consecutive exposures of 30 min each were recorded to increase the S/N ratio and remove cosmic ray hits. The adopted instrument set-up yielded a spectral resolution of about $R \approx 30\,000$. The data were reduced using standard IRAF routines. The wavelength solution was improved acquiring ThAr spectra immediately before and after each stellar observation. After accounting for instrumental shifts with telluric lines, the radial velocities were measured cross-correlating the target spectra with a spectrum of the RV standard star HR 5777 observed with the same instrument set-up.

As part of NASA's key science programme in support of the *CoRoT* mission, more RV measurements were obtained with the HIRES spectrograph (Vogt et al. 1994) mounted on the Keck I 10 m telescope, at the Keck Observatory (Mauna Kea, Hawai'i). With the aim of detecting the Rossiter-McLaughlin effect, 13 RV measurements were secured during the expected transit on 2009 July 1 (UT). The observations were performed with the red cross-disperser and the I_2 absorption cell to correct for instrumental shifts of the spectrograph. The $0\farcs861$ wide slit together with the $14''$ tall decker was employed to allow proper background subtraction, yielding a resolving power of $R \approx 50\,000$. In order to adequately sample the RM anomaly, the exposure time was set to 900 s. Two extra spectra of 1200 s each were also acquired out of transit, on 2009 June 30 (UT). The spectra were reduced with IRAF standard routines. The HIRES RV measurements were derived with the iodine data modelling code "Austral" (Endl et al. 2000).

The final RV measurements of CoRoT-11 are reported in Table 2, along with error bars, exposure times, and S/N ratio. In spite of the good RV stability of the spectrographs used in the present work, the relatively high $v \sin i_\star$ of CoRoT-11 strongly affected the RV precision of our measurements and led to an accuracy in the range ~100–200 m/s, with a typical error bar of about 100 m/s even for the HARPS and HIRES data. The five data-sets, i.e., the SOPHIE, HIRES, and TLS data, and the two HARPS modes, were simultaneously fitted with a Keplerian model, assuming a circular orbit. The HIRES RV measurements acquired during the transit were not used in the fit. Both period and transit central time were fixed according to the *CoRoT* ephemeris. An RV shift was let free to vary in the fit between the five data sets.

The RV measurements are plotted in Fig. 6 together with the best-fitting circular orbit. The derived orbital parameters are reported in Table 4, along with error bars that were computed from χ^2 variations and Monte Carlo experiments. The RV measurements led to a semi-amplitude $K = 280 \pm 40$ m/s. The standard deviation of the residuals to the fit is $\sigma_{\rm O-C} = 88$ m/s, in agreement with the expected accuracy of the RV measurements. The reduced χ^2 is 1.1 for the 22 RV measurements used in the fit.

We explored the possibility that the observed RV variations of CoRoT-11 do not result from the planet's orbital motion, but are instead caused by a periodic distortions in the spectral lines caused by either stellar magnetic activity or the presence of a hypothetical unresolved eclipsing binary, whose light is diluted by CoRoT-11. In order to exclude these scenarios, we performed an analysis of the cross-correlation function (CCF) profile. Using the highest resolution spectra in our data-set (i.e., the HARPS measurements) and following the line-bisector technique described in Queloz et al. (2001), we derived the difference in velocity space between the lower and upper part of the HARPS CCFs (i.e., bisector span). The value of the bisector span velocities are listed in Table 2. The uncertainty was set to twice that of the corresponding HARPS radial velocity measurements. We found that the CCFs show a systematic asymmetric profile, translating into a negative value of the bisector span velocities (Table 2 and Fig. 7), which is usually observed in rapidly rotating F-type stars (Gray 1986, 1989). Nevertheless, the CCF bisector spans show neither significant variations nor any trend as a function of both RV measurements and orbital phases (Fig. 7). The linear Pearson correlation coefficient between the HARPS RV measurements and the corresponding CCF bisector spans is −0.25. Removing the only outlier point with positive bisector span (i.e., 0.472 km s^{-1}), the correlation coefficient approaches zero, being −0.03. Thus the observed RV variations seem not to be caused by spectral line profile variations to any significant degree, but are mainly due to the Doppler shift induced by the orbital motion of CoRoT-11b. The RV observations and the transit-signal detected by *CoRoT* point to a hot-Jupiter-sized planet that orbits the star.

The phase-folded RV measurements are plotted in Fig. 8. As already described, the orbit was assumed to be circular, which is a reasonable assumption for close-in hot-Jupiters. The radial velocities are not accurate enough to constrain the eccentricity with the orbital fit only. Indeed, a Keplerian fit with an eccentricity of about 0.6 provides a solution that agrees with the *CoRoT* ephemeris, with a RV semi-amplitude K which is 15% larger than the one obtained for a circular orbit. The standard deviation of the residuals to this eccentric fit ($\sigma_{\rm O-C} = 95$ m/s) is marginally higher than the circular fit. Only extremely eccentric orbits with $e > 0.7$ produce low-quality fits, with dispersions larger than 120 m/s. Nevertheless, we put some constraints on the possible value for the planet eccentricity, taking advantage of the transit fit parameter $M_*^{1/3}/R_*$, from which the mean stellar density can be inferred (Sect. 2.2). The obtained value of $M_*^{1/3}/R_*$ depends on the eccentricity of the orbit. We found that for $e \gtrsim 0.2$ the mean stellar density would be incompatible with a F6 dwarf star, because it is significantly higher than the expected value (Cox 2000).

The on-transit RV data of CoRoT-11 are plotted in Fig. 9. Unfortunately, the HIRES observations were performed according to an old, slightly incorrect, transit ephemeris based on the analysis of the *alarm-mode* data only. Nevertheless, although the HIRES measurements cover only the first half of the transit, they clearly show that the Rossiter-McLaughlin (RM) anomaly has

Table 2. Radial velocities of the planet host star CoRoT-11 obtained with the SOPHIE, HARPS (EGGS and standard HARPS mode), COUDÉ@TLS, and HIRES spectrographs.

HJD (days)	RV (km s^{-1})	σ_{RV} (km s^{-1})	Bisector (km s^{-1})	Texp (s)	S/N per resolution element at 5500 Å
SOPHIE – HE Mode				$V_r = -0.920 \pm 0.160$	km s^{-1}
2454643.60252[a]	–1.164	0.218		1402	42
2454683.42036	–0.714	0.206		1607	50
HARPS – EGGS Mode				$V_r = -1.229 \pm 0.041$	km s^{-1}
2454731.52836	–0.932	0.067	–0.531	2700	88
2454742.51115	–1.364	0.104	–0.149	2700	54
2454745.51100	–1.370	0.087	–0.476	2700	66
2454746.51455	–0.986	0.071	–0.583	2700	81
2454747.51953	–1.509	0.115	–0.892	1800	48
HARPS – Standard Mode				$V_r = -1.336 \pm 0.044$	km s^{-1}
2455023.66206[a]	–1.663	0.149	–0.286	3600	34
2455024.63997[a]	–1.405	0.111	–0.705	3600	48
2455045.69605[a]	–1.013	0.114	–0.747	3600	52
2455064.60739	–1.166	0.083	–0.408	3300	64
2455067.51277	–1.085	0.092	–0.204	3300	59
2455068.49041	–1.547	0.130	0.472	3300	42
2455069.51299	–1.384	0.110	–0.497	3300	48
COUDÉ@TLS				$V_r = -0.640 \pm 0.130$	km s^{-1}
2455035.46055	–0.951	0.174		2×1800	25
2455057.40390	–0.541	0.175		2×1800	25
HIRES				$V_r = -0.207 \pm 0.040$	km s^{-1}
2455012.80417	–0.033	0.050		1200	61
2455013.06216	0.181	0.086		1200	71
2455013.78975	–0.165	0.089		900	54
2455013.80073	–0.083	0.090		900	56
2455013.81181	–0.170	0.135		900	56
2455013.82275	0.173	0.111		900	57
2455013.83360	–0.012	0.142		900	57
2455013.84473	0.099	0.073		900	56
2455013.85572	0.037	0.119		900	56
2455013.86677	0.274	0.108		900	55
2455013.87785	0.240	0.078		900	55
2455013.88881	0.017	0.100		900	56
2455013.89978	0.089	0.080		900	56
2455013.91097	–0.263	0.086		900	54
2455014.05389	–0.386	0.119		900	58

Notes. The systemic velocities for each instrument, as derived from the circular Keplerian fit to the data, are reported on the right of the listed spectrographs. The footnote indicates the RV measurements that have been corrected for moonlight contamination. [(a)] Corrected for moonlight contamination.

been detected, which also confirms the occurrence of the transit events. The RM amplitude is large (~400 m/s), because of the fast stellar rotation. This also proves that the transiting object has a planetary size. The first part of the spectroscopic transit shows radial velocities that are blue-shifted compared to the Keplerian fit, which clearly indicates that the orbit is prograde. In addition, systematics seem to be present in the data at a level above the expected uncertainties for some measurements. It is thus difficult to constrain the spin-orbit angle with the current data. In Fig. 9 we show a model with $\lambda = 0°$ and $v \sin i_\star = 40$ km s^{-1}, using the analytical approach developed by Ohta et al. (2005). The fit is not satisfying, suggesting in particular a $v \sin i_\star$ value higher than the one we derived from the SOPHIE RV data and the spectral analysis (Sect. 3.4), in order to have a larger amplitude for the anomaly. It is known that a discrepancy could be found between the $v \sin i_\star$ values measured from the RM effect and from the spectral modelling of line broadening, especially for fast rotators (see e.g., Simpson et al. 2010). Concerning the spin-orbit angle, the data are compatible with $\lambda = 0°$. However, as for $v \sin i_\star$, the moderate quality of the data-set prohibits accurate measurements. Additional RM observations of CoRoT-11 should be performed, with a full coverage of the event.

3.4. High-resolution spectroscopy and stellar analysis

To derive the fundamental atmospheric parameters of the planet host star, we observed CoRoT-11 with the high-resolution spectrograph UVES mounted at the 8.2 m Very Large Telescope (ESO-VLT; Paranal Observatory, Chile). Two consecutive spectra of 2380 s each were acquired in service mode on 2008 September 17, under the ESO programme 081.C-0413(C). The star was observed through a 0.″5 wide slit, setting the UVES spectrograph to its Dic-1 mode (346+580). The adopted configuration yielded a resolving power of about 65 000, with a spectral coverage $\lambda \approx 3000-6800$ Å. The spectra were extracted and combined with standard IRAF packages, giving a final S/N ratio of about 160 at 5500 Å.

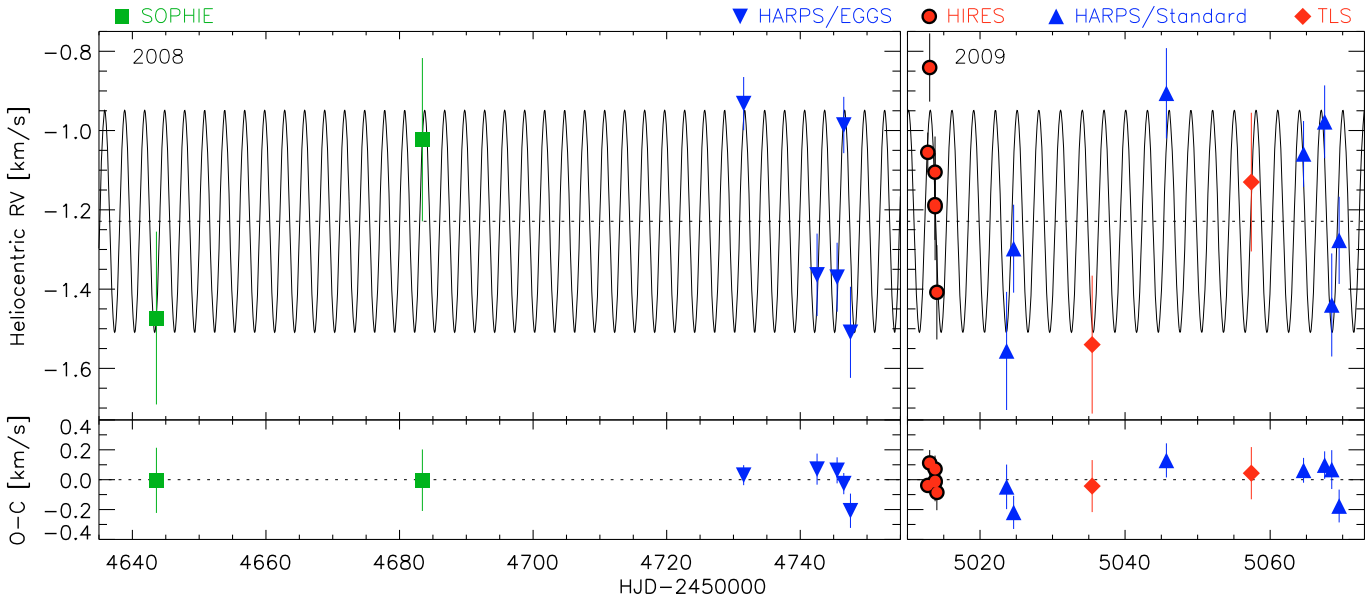

Fig. 6. *Top*: radial velocity measurements of CoRoT-11 with 1-σ error bars as a function of time and the Keplerian fit to the data. The data are from SOPHIE (green squares), HARPS (blue downward and upward triangles for EGGS and HARPS modes, respectively), HIRES (red circles), and COUDÉ@TLS (red diamonds). The *left and right panels* show the two observational seasons in 2008 and 2009. The systemic radial velocity of $V_r = -1.229 \pm 0.041$ km s^{-1}, as derived from the HARPS/EGGS data-set only, is plotted with a horizontal dotted line. *Bottom*: residuals of the fit.

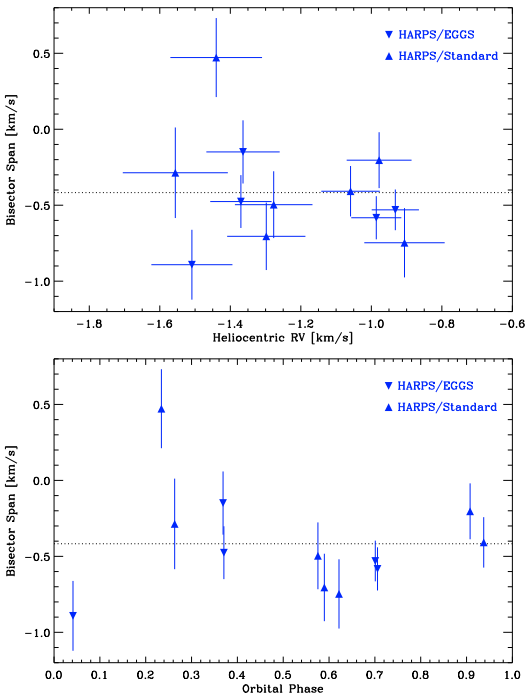

Fig. 7. Bisector spans versus radial velocity measurements (*top panel*) and orbital phases (*bottom panel*) as derived from the HARPS data (blue downward and upward triangles for EGGS and HARPS modes, respectively). The horizontal dotted line marks the average negative value of the CCF bisector span, i.e. −0.417 km s^{-1}.

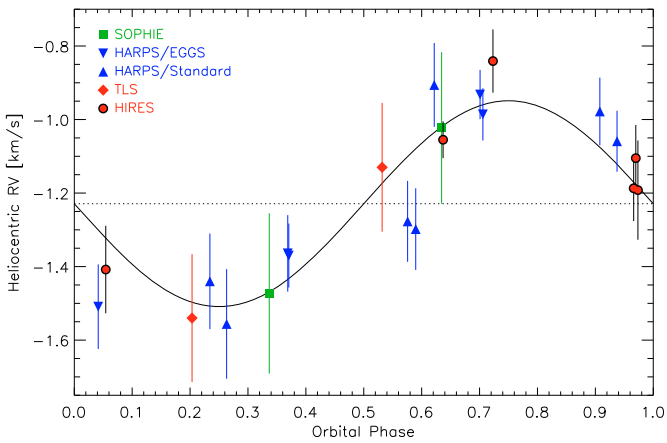

Fig. 8. Phase-folded radial velocity measurements of CoRoT-11, and Keplerian fit to the data. The horizontal dotted line marks the systemic radial velocity $V_r = -1.229 \pm 0.041$ km s^{-1}, as derived from the HARPS/EGGS data-set only.

The effective temperature ($T_{\rm eff}$), surface gravity ($\log g$), metallicity ([Fe/H]), and projected rotational velocity ($v \sin i_\star$) of CoRoT-11 were derived following the procedure already adopted for other *CoRoT* host stars (e.g., Deleuil et al. 2008; Fridlund et al. 2010; Bruntt et al. 2010). We took advantage of different spectral analysis packages applied independently by different teams within the *CoRoT* community, e.g., the SME 2.1 (Valenti & Piskunov 1996; Valenti & Fischer 2005), the VWA (Bruntt et al. 2004; Bruntt et al. 2008, 2010) software. We found that the estimated values of the above mentioned physical parameters agree within the error bars. The final adopted values are $T_{\rm eff} = 6440 \pm 120$ K, $\log g = 4.22 \pm 0.23$, [Fe/H] $= -0.03 \pm 0.08$, and $v \sin i_\star = 40 \pm 5$ km s^{-1} (Table 4), with the latter value in perfect agreement with the one derived from the RV data (Sect. 3.3).

We also used the VWA software package to perform a detailed abundance analysis of the UVES spectrum of CoRoT-11, by iteratively fitting reasonably isolated spectral lines. Atmosphere models were interpolated in a grid of MARCS models (Gustafsson et al. 2008) and atomic data were extracted from VALD (Kupka et al. 1999). However, owing to the relatively high $v \sin i_\star$ of the star, only 71 lines turned out to be sufficiently isolated and thus suitable for spectral analysis.

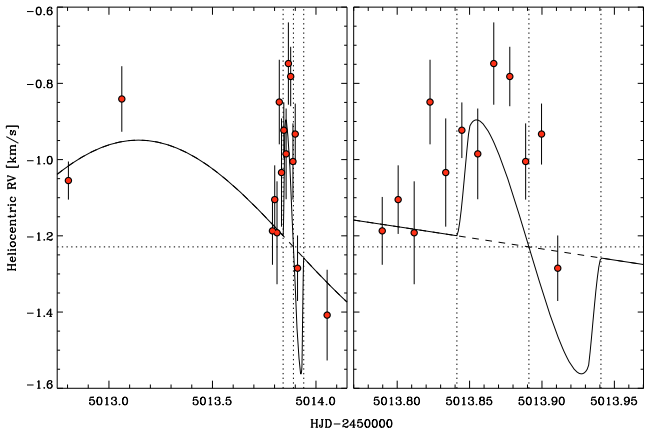

Fig. 9. Radial velocities of CoRoT-11 measured with the HIRES spectrograph around the transit that occurred on July 1, 2010. The *left panel* shows all the RV data and the *right panel* shows a magnification on the transit. The dashed line shows the Keplerian fit without transit. The solid line shows the Rossiter-McLaughlin anomaly fit for $\lambda = 0°$. The vertical dotted lines show the transit first contact, mid-time, and fourth contact. The data have been arbitrarily shifted to the systemic radial velocity of $V_r = -1.229 \pm 0.041$ km s^{-1} (horizontal dotted line), as derived from the HARPS/EGGS data-set only.

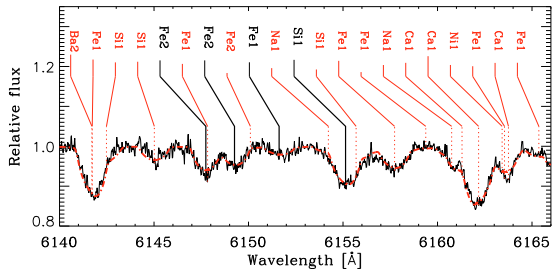

Fig. 10. Small section of the observed UVES spectrum (thin black line) together with the best-fitting synthetic template (dashed line). The spectral lines used for the abundance analysis and the neighbouring lines are shown with black and red colours, respectively. See the online edition of the Journal for a colour version of this figure.

A small section of the observed and fitted synthetic spectra is shown in Fig. 10. Abundances were computed relative to the Sun to correct the oscillator strengths (see Bruntt et al. 2008; Bruntt 2009). We determined the atmospheric parameters by adjusting them to minimise the correlation of iron (Fe) with equivalent width (EW) and excitation potential (EP). Furthermore, we required that Fe I and Fe II have the same mean abundance within the uncertainty. To evaluate the uncertainty on the atmospheric parameters, we perturbed them to determine when the correlations of Fe I with EW or EP become significant or the Fe I and Fe II abundances deviate by more than 1 σ (see Bruntt et al. 2008, for details). In Table 3 we list the abundances relative to the Sun for the five elements Na, Si, Ca, Fe, and Ni.

Table 3. Abundances relative to the Sun for five elements in CoRoT-11.

Element	[A/H]	N
Na I	-0.10 ± 0.15	2
Si I	0.10 ± 0.09	5
Si II	0.19 ± 0.18	2
Ca I	0.03 ± 0.12	4
Fe I	-0.04 ± 0.08	44
Fe II	-0.02 ± 0.08	6
Ni I	-0.08 ± 0.11	8

Notes. The number of spectral lines used in the VWA abundance analysis are given in the last column.

4. Results

4.1. Stellar parameters of the parent star CoRoT-11

To determine the mass and radius of the CoRoT-11 host star we took advantage of the stellar parameter $(M_*^{1/3}/R_*)$ as derived from the *CoRoT* light curve analysis (Sect. 2.2), and of the effective temperature and metallicity ($T_{\rm eff}$ and [Fe/H]) as obtained from the spectral analysis (Sect. 3.4). We thus compare the location of the star on a $\log(M_*^{1/3}/R_*)$ vs. $\log(T_{\rm eff})$ H-R diagram with evolutionary tracks computed with the CESAM code (Morel & Lebreton 2008). According to these theoretical models we obtained a stellar mass of $M_\star = 1.27 \pm 0.05\ M_\odot$ and a stellar radius of $R_\star = 1.37 \pm 0.03\ R_\odot$, with an age of about 2.0 ± 1.0 Gyr (Table 4). From these results we derived a surface gravity of $\log g = 4.26 \pm 0.06$, in good agreement with the spectroscopically determined value of $\log g = 4.22 \pm 0.23$. We also checked whether the high rotation rate of the star can account for a significant flattening at the poles. According to the equation by Claret (2000) and assuming that the star is seen almost edge-on, the equatorial and polar radii should differ by only ~0.6%, making the flattening effect negligible.

We computed the interstellar extinction to the star following the general guidelines described in Gandolfi et al. (2008). The seven $BVr'i'JHKs$ broad-band magnitudes as retrieved from the *ExoDat* database enabled us to construct the spectral energy distribution (SED) of CoRoT-11, covering a wide spectral range, from optical to near-infrared wavelengths (see Table 1). Simultaneously using all the photospheric colours encompassed by the SED, we derived the interstellar extinction to the star ($A_{\rm V}$) by fitting the observed SED with a theoretical one progressively reddened with an increasing value of $A_{\rm V}$. The theoretical SEDs were computed with the *NextGen* stellar atmosphere model (Hauschildt et al. 1999) with the same $T_{\rm eff}$, $\log g$, and [Fe/H] as the star, the response curve of the *ExoDat* photometric system, and the extinction law by Cardelli et al. (1989). Assuming a total-to-selective extinction $R_{\rm V} = A_{\rm V}/E_{\rm B-V} = 3.1$ (typical of the diffuse interstellar medium in our Galaxy), as well as a black body emission at the star's effective temperature and radius, we derived an extinction $A_{\rm V} = 0.55 \pm 0.10$ mag and a distance to the star $d = 560 \pm 30$ pc (Table 4).

We attempted to derive the rotation period of the star from the *CoRoT* light curve. The Lomb-Scargle periodogram (Scargle 1982) applied to the out-of transit data-points shows only one significant broad peak at about 8.5 ± 2 days, with a light curve amplitude of ~0.25%. This period is not compatible with the maximum rotation period of 1.73 ± 0.22 days derived from the projected rotational velocity and radius of the planet host star. The detected signal at 8.5 ± 2 days might be due to a 0.02 mag periodic variation of the nearby contaminant star located at about 2″ from CoRoT-11 (see Sects. 2.2 and 3.1). On the other hand, a low-level of magnetic activity of CoRoT-11 might account for no significant signals at $\lesssim$2.0 days, as confirmed from the absence of emission features in the core of the Ca II H & K and Balmer lines.

Table 4. CoRoT-11b – Planet and star parameters.

Ephemeris	
Planet orbital period P [days]	2.994330 ± 0.000011
Planetary transit epoch $T_{\rm tr}$ [HJD-2 400 000]	54597.6790 ± 0.0003
Planetary transit duration $d_{\rm tr}$ [h]	2.5009 ± 0.0144
Results from radial velocity observations	
Orbital eccentricity e	0 (fixed)
Radial velocity semi-amplitude K [m/s]	280.0 ± 40.0
O–C residuals [m/s]	88
Fitted transit parameters	
Planet-to-star radius ratio $k = R_{\rm p}/R_*$	0.1070 ± 0.0005
Linear limb darkening coefficient u_+	0.61 ± 0.06
Linear limb darkening coefficient u_-	0.02 ± 0.04
Orbital phase of planetary transit ingress (θ_1)	−0.0174 ± 0.0001
Deduced transit parameters	
Scaled semi-major axis a/R_*	6.890 ± 0.080
$M_*^{1/3}/R_*$ [solar units]	0.787 ± 0.010
Mean stellar density ρ_* [g/cm^3]	0.69 ± 0.02
Inclination i [deg]	83.170 ± 0.150
Impact parameter[a] b	0.818 ± 0.008
Spectroscopic parameters	
Effective temperature $T_{\rm eff}$ [K]	6440 ± 120
Surface gravity log g[b] [dex]	4.22 ± 0.23
Surface gravity log g[c] [dex]	4.26 ± 0.06
Metallicity [Fe/H] [dex]	−0.03 ± 0.08
Stellar rotational velocity $v \sin i_\star$ [km s^{-1}]	40.0 ± 5.0
Spectral type	F6 V[d]
Stellar physical parameters from combined analysis	
Star mass $M_\star$ [$M_\odot$]	1.27 ± 0.05
Star radius $R_\star$ [$R_\odot$]	1.37 ± 0.03
Age of the star t [Gyr]	2.0 ± 1.0
Interstellar extinction $A_{\rm V}$ [mag]	0.55 ± 0.10
Distance of the system d [pc]	560 ± 30
Planetary physical parameters from combined analysis	
Planet mass $M_{\rm p}$ [$M_{\rm J}$][e]	2.33 ± 0.34
Planet radius $R_{\rm p}$ [$R_{\rm J}$][e]	1.43 ± 0.03
Planet density $\rho_{\rm p}$ [g/cm^3]	0.99 ± 0.15
Orbital semi-major axis[a] [AU]	0.0436 ± 0.005
Equilibrium temperature[f] $T_{\rm eq}$ [K]	1657 ± 55

Notes. [(a)] The impact parameter is defined as $b = \frac{a \cdot \cos i}{R_*}$; [(b)] derived from the spectroscopic analysis; [(c)] derived using the light curve parameter $M_*^{1/3}/R_*$ and the stellar mass as inferred from stellar evolutionary models; [(d)] with an accuracy of ± 1 sub-class; [(e)] radius and mass of Jupiter taken as 71 492 km and 1.8986×10^{30} g, respectively; [(f)] zero albedo equilibrium temperature for an isotropic planetary emission.

4.2. Planetary parameters of CoRoT-11b

Based on the stellar mass and radius (Sect. 4.1), the RV curve semi-amplitude (Sect. 3.3), the planet-to-star radius ratio, and the planet orbit inclination (Sect. 2.2), we derived a mass for CoRoT-11b of $M_{\rm p} = 2.33 \pm 0.34\ M_{\rm Jup}$ and a radius of $R_{\rm p}$= $1.43 \pm 0.03\ R_{\rm Jup}$, yielding a mean planetary density $\rho_{\rm p} = 0.99 \pm 0.15$ g/cm^3. The planet orbits its host star at a distance of $a = 0.0436 \pm 0.005$ AU in 2.994339 ± 0.000011 days. The planetary mass has been obtained assuming an eccentricity $e = 0$. According to the results presented in Sect. 3.3, we cannot exclude a slightly eccentric orbit, with $0 \lesssim e \lesssim 0.2$. Nevertheless, for $e = 0.2$ the planetary mass would decrease of about 4%, i.e., well within the error bar of our estimation. A summary of the planetary parameters derived in the present work is reported in Table 4.

5. Discussion

Together with 30 Ari Bb (Guenther et al. 2009), OGLE2-TR-L9b (Snellen et al. 2009), and WASP-33b (Collier Cameron et al. 2010) orbiting a F6 V ($v \sin i_\star$ = 39 km s^{-1}), F3 V ($v \sin i_\star$ = 39.3 km s^{-1}), and A5 V star ($v \sin i_\star = 90 \pm 10$ km s^{-1}), respectively, CoRoT-11b is the fourth extrasolar planet discovered around a rapidly rotating main sequence star ($v \sin i_\star = 40 \pm 5$ km s^{-1}; see Fig. 11). Furthermore, the planet host star CoRoT-11, with its effective temperature of $T_{\rm eff} = 6440 \pm 120$ K, is one of the hottest stars known to harbour an extrasolar planet.

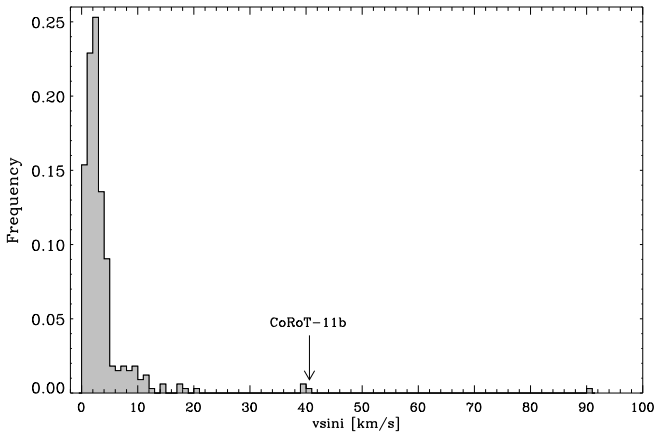

Fig. 11. $v \sin i_\star$ distribution of the known extrasolar planets. The position of CoRoT-11b is highlighted with an arrow.

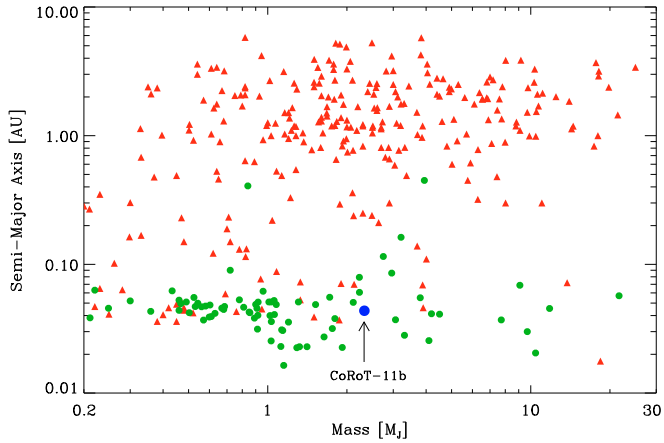

Fig. 12. Semi-major axis versus planetary mass for the known extrasolar planets detected in radial velocity (triangles) and transit surveys (circles). The position of CoRoT-11b is highlighted with an arrow.

Most of the bulk of known extrasolar planets have been detected with the RV method. Although this technique has dramatically increased the number of discoveries in the last fifteen years, it suffers from a strong selection bias, because it is mostly restricted to planets around slowly rotating stars ($v \sin i_\star \lesssim 10$ km s^{-1}). This observational bias limits our knowledge of extrasolar planets to mainly late-type solar-like stars. One of the big advantages of the transit method is that it is insensitive to the stellar rotation, enabling us to single out planets even around intermediate-mass stars (Collier Cameron et al. 2010). This allows us to enlarge the parameter space of planet host stars and gives us a chance to study the planet formation around A and F stars. Even if CoRoT-11b has been confirmed and studied thanks to a complementary and intensive RV campaign, it would have likely been rejected from any RV search sample because of the fast rotation of its parent star. Indeed, about 20 RV measurements were needed to assess the planetary nature of CoRoT-11b and constrain its mass within ∼15%. But the RV signature of CoRoT-11b has been detected because of its high mass. Taking into account the accuracy of our RV measurements (100–200 m/s), if the mass of CoRoT-11b had been $M_p \lesssim 0.5\ M_{Jup}$, it would not have been detected by the RV survey.

According to our planetary mass determinations ($M_p = 2.33 \pm 0.34$), CoRoT-11b is among the most massive transiting hot-Jupiters discovered so far. It actually belongs to the poorly populated sub-group of objects with planetary masses around 2 M_{Jup}. As already noticed by Torres et al. (2010), there seems to be a lack of transiting hot-Jupiters with masses larger than about 2 M_{Jup}. Based on the list of currently known transiting planets[6], hot-Jupiters with masses in the range $0.5 \lesssim M_p \lesssim 1.5\ M_{Jup}$ seem to be ∼5 times more numerous than those with masses $1.5 \lesssim M_p \lesssim 2.5\ M_{Jup}$. This trend is also confirmed by the number of planets discovered with the RV method. In Fig. 12 the semi-major axis of the planets detected in radial velocity and transit surveys is plotted as a function of the planetary mass. Let us consider only the objects with $a \lesssim 0.1$ AU and $M_p \gtrsim 0.2\ M_{Jup}$, i.e., hot-Saturn and Jupiter planets. There is a clear clump of hot-giant planets with masses between the mass of Saturn (∼0.30 M_{Jup}) and Jupiter, orbiting their parent star at about 0.04–0.06 AU. Starting from ∼1.0 M_{Jup}, the number of hot-Jupiters seems to drop off, whereas the spread in the semi-major axis increases. For $M_p \gtrsim 2\ M_{Jup}$ the number of hot-Jupiters falls off significantly. The same trend is not seen for planets with $1 \lesssim a \lesssim 5$ AU. The lack of Saturn planets orbiting their parent at such a distance might be owing to an observational bias of the RV technique. Nevertheless, since both the Doppler and transit methods are strongly sensitive in detecting close-in massive planets, we conclude that hot-Jupiters with $M_p > 2\ M_{Jup}$ are significantly less common than "normal" hot-Saturn and Jupiter planets.

By assuming that CoRoT-11b is a hydrogen-rich gas giant we estimated the planet's thermal mass loss by applying the method outlined in detail in Lammer et al. (2009). Because the planet orbits a F6-type star with an age between 1.0 and 3.0 Gyr, we used the soft X-rays and EUV flux scaling law of Eq. (12) of Lammer et al. (2009) and integrated the thermal mass loss during the planet's history up to the two age values given above. By using the stellar and planetary parameters and a heating efficiency η for hydrogen-rich thermospheres, which can be considered between 10–25% (Lammer et al. 2009; Murray-Clay et al. 2009), we obtained a present time mass loss rate for CoRoT-11b of about 2.0×10^{10} g/s or an integrated loss of 0.07% of its present mass ($\eta = 10\%$), and about 5.0×10^{10} g/s, or 0.18% ($\eta = 25\%$) if the host star and planet are 1.0 Gyr old. If the the star/planet system is 3.0 Gyr old, we estimated a mass loss rate of about 3.0×10^9 g/s, or 0.1% ($\eta = 10\%$) and about 7.7×10^9 g/s, or 0.25% ($\eta = 25\%$) during the planet lifetime. These loss rates agree well with hydrodynamic escape model results for typical hot Jupiters (Yelle et al. 2008). Although the planet radius is $1.43 \pm 0.03\ R_{Jup}$, the main reason why the thermal mass loss of CoRoT-11b is not significant is related to the large mass of the planet of $2.33 \pm 0.34\ M_{Jup}$. According to Lammer et al. (2009), only hot gas giant planets with $\rho_p \ll 1$ g/cm^3 should experience large thermal mass loss.

In order to investigate whether a standard model for an irradiated planet can account for the density of CoRoT-11b, we computed stellar and planetary evolution models using CESAM (Morel & Lebreton 2008) and CEPAM (Guillot & Morel 1995), as described in Bordé et al. (2010) and Guillot & Havel (2010). The results are shown in Fig. 13 where the evolution of the size of CoRoT-11b is plotted as a function of the system age. The colours indicate the distance in standard deviations from the inferred effective temperature and mean stellar density, i.e.,

[6] We refer the reader to the Extra Solar Planets Encyclopedia for a constantly updated list of known extra solar planets (http://exoplanet.eu/).

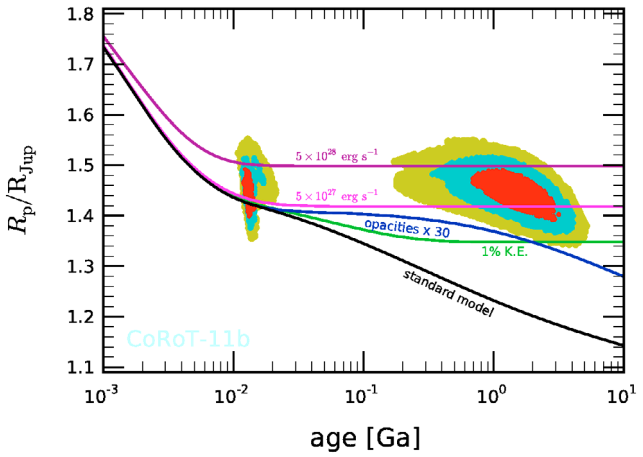

Fig. 13. Evolution of the size of CoRoT-11b (in Jupiter units, 1 R_{Jup} = 71 492 km) as a function of the age of the system (in Ga = 10^9 years). The coloured areas correspond to constraints derived from stellar evolutionary models matching the mean stellar density and effective temperature within a certain number of standard deviations: less than 1σ (red), 2σ (blue) or 3σ (green). The curves are evolutionary tracks for CoRoT-11b computed assuming a planetary mass of $M = 2.33\ M_{Jup}$ and equilibrium temperature T_{eq} = 1657 K), and using different models as labelled (see text for more details and the online edition of the Journal for a colour version of this figure).

less than 1σ (red), 2σ (blue) or 3σ (green). These constraints are compared to planetary evolution models for a homogeneous solar-composition hydrogen-planet, with different hypotheses: (1) using a "standard model", i.e., without additional sources of heat; (2) by increasing interior opacities by a factor 30; (3) by adding a fraction (∼1%) of the incoming stellar energy and dissipating it at the centre; (4) and (5) by dissipating 5×10^{27} and 5×10^{28} erg/s at the centre of the planet. The first three cases correspond to standard recipes used to explain the inflated giant exoplanets (Guillot 2008). The last two cases correspond to higher dissipation levels that are required to explain the planet size for the oldest ages.

Interestingly, as for CoRoT-2b (Guillot & Havel 2010), two classes of solutions are found: (i) the standard solution for which the host star is on the main sequence (with an age of about 2.0 ± 1.0 Gyr) and the planet requires a high level of dissipation in its interior in order to account for its large size; (ii) a very young class of solutions in which the star is still on the pre-main sequence (PMS) phase (with an age of about 12 ± 2 Myr) and the planet size can be quite naturally explained with a "standard model". However, the latter scenario is in contradiction with the absence of the detectable Li I λ6708 Å line in the spectra of CoRoT-11. According to our effective temperature determination (T_{eff} = 6440 ± 120 K), CoRoT-11 would belong to the narrow class of F-stars, which have suffered strong surface lithium depletion during the first billion years of their life. Indeed, studies of the lithium content in the photosphere of F-type stars in galactic clusters and field stars have revealed the presence of a narrow dip in the lithium abundance for effective temperature between 6500 and 6800 K (Mallik et al. 2003; Böhm-Vitense 2004). While the so-called "lithium-dip" is absent in the Pleiades (Pilachowski et al. 1987) and in general in all the young cluster ($\lesssim$100 Myr), this dip is well observed in older cluster like the Hyades (700 Myr; Boesgaard & Tripicco 1986a), NGC 752 (1.7 Gyr; Hobbs & Pilachowski 1986), as well as in many field F-stars (e.g., Boesgaard & Tripicco 1986b). We thus believe that an age of 2.0 ± 1.0 Gyr is more plausible for the planet-star system.

Acknowledgements. We thank the anonymous referee for his/her careful reading, useful comments, and suggestions, which helped to improve the manuscript. This paper is based on observations carried out at the European Southern Observatory (ESO), La Silla and Paranal (Chile), under observing programs numbers 081.C-0388, 081.C-0413, and 083.C-0186. The authors are grateful to the staff at ESO La Silla and ESO Paranal Observatories for their support and contribution to the success of the HARPS and UVES observing runs.
This paper is also based on observations performed with SOPHIE at the Observatoire de Haute-Provence, France, under observing program PNP.08A.MOUT.
Part of the data presented herein were obtained at the W.M. Keck Observatory from telescope time allocated to the National Aeronautics and Space Administration through the agency's scientific partnership with the California Institute of Technology and the University of California. The Observatory was made possible by the generous financial support of the W.M. Keck Foundation. The authors wish to recognize and acknowledge the very significant cultural role and reverence that the summit of Mauna Kea has always had within the indigenous Hawaiian community. We are most fortunate to have the opportunity to conduct observations from this mountain.
The team at IAC acknowledges support by grant ESP2007-65480-C02-02 of the Spanish Ministerio de Ciencia e Innovacion. The German *CoRoT* Team (TLS and the University of Cologne) acknowledges DLR grants 50OW0204, 50OW0603, and 50QP07011.
This research has made use of the SIMBAD database, operated at CDS, Strasbourg, France.

References

Aigrain, S., Collier Cameron, A., Ollivier, M., et al. 2008, A&A, 488, 43
Aigrain, S., Pont, F., Fressin, F., et al. 2009, A&A, 506, 425
Alonso, R., Auvergne, M., Baglin, A., et al. 2008, A&A, 482, L21
Alonso, R., Guillot, T., Mazeh, T., et al. 2009a, A&A, 501, L23
Alonso, R., Alapini, A., Aigrain, S., et al. 2009b, A&A, 506, 353
Anderson, D. R., Hellier, C., Gillon, M., et al. 2010, ApJ, 709, 159
Auvergne, M., Bodin, P., Boisnard, L., et al. 2009, A&A, 506, 411
Baglin, A., Auvergne, M., Boisnard, L., et al. 2006, 36th COSPAR Scientific Assembly, 36, 3749
Böhm-Vitense, E. 2004, AJ, 128, 2435
Baranne, A., Queloz, D., Mayor, M., et al. 1994, A&AS, 119, 373
Barge, P., Baglin, A., Auvergne, M., et al. 2008, A&A, 482, L17
Boesgaard, A. M., & Tripicco, M. J. 1986, ApJ, 302, 49
Boesgaard, A. M., & Tripicco, M. J. 1986b, ApJ, 303, 724
Bordé, P., Bouchy, F., Deleuil, M., et al. 2010, A&A, 520, A66
Borucki, W. J., & Summers, A. L. 1984, Icarus, 58, 121
Borucki, W. J., Koch, D. G., Brown, T. M., et al. 2010, ApJ, 713, L126
Bouchy, F., Queloz, D., Deleuil, M., et al. 2008, A&A, 482, L25
Bouchy, F., Hébrard, G., Udry, S., et al. 2009, A&A, 505, 853
Bowler, B. P., Johnson, J. A., Marcy, G. W., et al. 2010, ApJ, 709, 396
Bruntt, H. 2009, A&A, 506, 235
Bruntt, H., Bikmaev, I. F., Catala, C., et al. 2004, A&A, 425, 683
Bruntt, H., De Cat, P., & Aerts, C. 2008, A&A, 478, 487
Bruntt, H., Deleuil, M., Fridlund, M., et al. 2010, A&A, 519, A51
Cabrera, J., Fridlund, M., Ollivier, M., et al. 2009, A&A, 506, 501
Collier Cameron, A., Günther, E., Smalley, B., et al. 2010, MNRAS, 407, 507
Carpano, S., Cabrera, J., Alonso, R., et al. 2009, A&A, 506, 491
Cardelli, J. A., Clayton, G. C., & Mathis, J. S. 1989, ApJ, 345, 245
Carone, L., Gandolfi, D., et al., A&A, submitted
Claret, A. 2000, A&A, 359, 289
Cox, A. N. 2000, Allen's astrophysical quantities, ed. A.N. Cox, 4th edn., AIP Press
Cresswell, P., Dirksen, G., Kley, W., & Nelson, R.P. 2007, A&A, 473, 329
Cutri R. M., Skrutskie M. F., van Dyk, S., et al. 2003, 2MASS All-Sky Catalog of Point Sources, NASA/IPAC Infrared Science Archive
Deeg, H. J., Gillon, M., Shporer, A., et al. 2009, A&A, 506, 343
Deeg, H. J., Moutou, C., Erikson, A., et al. 2010, Nature, 464, 384
Deleuil, M., Deeg, H. J., Alonso, R., et al. 2008, A&A, 491, 889
Deleuil, M., Meunier, J. C., Moutou, C., et al. 2009, AJ, 138, 649
Eigmüller, P., & Eislöffel, J. 2009, Transiting Planets, Proceedings of the International Astronomical Union, IAU Symp. Trasiting Planet, 253, 340
Eislöffel, J., Hatzes, A. P., Rauer, H., et al. 2007, Solar and Stellar Physics Through Eclipses ASP Conf. Ser., 370, 91
Endl, M., Kürster, M., Els, S. 2000, A&A, 362, 585
Frasca A., Alcalá, J. M., Covino, E., et al. 2003, A&A, 405, 149

Fridlund, M., Hebrard, G., Alonso, R., et al. 2010, A&A, 512, A14
Gandolfi, D., Alcalá, J. M., Leccia, S., et al. 2008, ApJ, 686, 1303
Gaudi, B. S., & Winn J. N. 2007, ApJ, 655, 550
Guenther, E. W., Hartmann, M., Esposito, M., et al. 2009, A&A, 507, 1659
Guillot, T. 2008, Phys. Scrip., 130, 014023
Guillot, T., & Morel, P. 1995, A&AS, 109, 109
Guillot, T., & Havel, M. 2010, A&A, in press [DOI:10.1051/0004-6361/201015051]
Gray D. F. 1986, PASP, 98, 319
Gray D. F. 1989, PASP, 101, 832
Giménez, A. 2006, A&A, 450, 1231
Gustafsson, B., Edvardsson, B., Eriksson, K., et al. 2008, A&A, 486, 951
Hauschildt, P. H., Allard, F., & Baron, E. 1999, ApJ, 512, 377
Hébrard, G., Bouchy, F., Pont, F., et al. 2008, A&A, 481, 52
Hobbs, L. M., & Pilachowski, C. 1986, ApJ, 309, 17
Johnson, J. A., Howard, A. W., Bowler, B. P., et al. 2010, PASP, 122, 701
Kallrath, J., & Milone, E.F. 2009, Eclipsing Binary Stars: Modeling and Analysis (New York: Springer-Verlag)
Koch, D. G., Borucki, W. J., Basri, G., et al. 2010, ApJ, 713, L79
Kupka, F., Piskunov, N., Ryabchikova, T. A., Stempels, H. C., & Weiss, W. W. 1999, A&AS, 138, 119
Lammer, H., Odert, P., Leitzinger, M., et al. 2009, A&A, 506, 399
Lagrange, A.-M., Desort, M., Galland, F., et al. 2009, A&A, 495, 335
Léger, A., Rouan, D., Schneider, J., et al. 2009, A&A, 506, 287
Lubow, S. H., & Ogilvie, G. I. 2001, ApJ, 560, 997
Mayor, M., & Queloz, D. 1995, Nature, 378, 355
Mayor, M., Pepe, F., Queloz, D., et al. 2003, Msngr., 114, 20
Mallik, S. V., Parthasarathy, M., & Pati, A. K. 2003, A&A, 409, 251M
Morel, P., & Lebreton, Y. 2008, Ap&SS, 316, 61
Moutou, C., Bruntt, H., Guillot, T., et al. 2008, A&A, 488, L47
Moutou, C., Hébrard, G., Bouchy, F., et al. 2009a, A&A, 498, L5
Moutou, C., Pont, F., Bouchy, F., et al. 2009b, A&A, 506, 321
Murray-Clay, R. A., Chiang, E. I., & Murray, N. 2009, ApJ, 693, 23
O'Toole, S. J., Tinney, C. G., Jones, H. R. A., et al. 2009, MNRAS, 392, 641
Ohta, Y., Taruya, A., & Suto, Y. 2005, ApJ, 622, 1118
Papaloizou, J. C. B., & Terquem, C. 2006, Rep. Prog. Phys., 69, 119
Pepe, F., Mayor, M., Galland, F., et al. 2002, A&A, 388, 632
Pilachowski, C. A., Booth, J., & Hobbs, L. M. 1987, PASP, 99, 1288
Pinheiro da Silva, L., Rolland, G., Lapeyrere, V., & Auvergne, M. 2008, MNRAS, 384, 1337
Pollacco, D., Skillen, I., Collier Cameron, A., et al. 2007, MNRAS, 385, 1576
Pont, F., Endl, M., Cochran, W. D., et al. 2009, MNRAS, 402, 1
Press, W. H., Teukolsky, S. A., Vetterling, W. T., & Flannery, B. P. 1992, Numerical recipes in C. The art of scientific computing (Cambridge: University Press), 2nd edn
Queloz, D., Henry, G. W., Sivan, J. P., et al. 2001, A&A, 379, 279
Queloz, D., Bouchy, F., Moutou, C., et al. 2009, A&A, 506, 303
Quentin, C. G., Barge, P., Cautain, R., et al. 2006, in ESA SP, 1306, 409
Rauer, H., Queloz, D., Csizmadia, S., et al. 2009, A&A, 506, 281
Rosenblatt, F. 1971, Icarus, 14, 71
Scargle, J. D. 1982, ApJ, 263, 835
Seager, S., & Mallén-Ornelas, G. 2003, ApJ, 585, 1038
Simpson, E. K., Pollacco, D., Hébrard, G., et al. 2010, MNRAS, 405, 1867
Sing, D. K. 2010, A&A, 510, A21
Snellen, I. A. G., Koppenhoefer, J., van der Burg, R. F. J., et al. 2009, A&A, 497, 545
Surace, C., Alonso, R., Barge, P., et al. 2008, SPIE, 7019, 111
Torres, G., Bakos, G.Á., Hartman, J., et al. 2010, ApJ, 715, 458
Valenti, J. A., & Piskunov, N. 1996, A&AS, 118, 595
Valenti, J. A., & Fischer, D. A. 2005, ApJS, 159, 141
Vogt, S. S., Allen, S. L., & Bigelow, B. C., et al. 1994, SPIE, 2198, 362
Winn J. N. 2010, in exoplanets, ed. S. Seager, Space Science Series, (University of Arizona: Press) in press [arXiv:1001.2010]
Yelle, R., Lammer, H., & Ip, W.-H. 2008, Space Sci. Rev., 139, 437

[1] Thüringer Landessternwarte, Sternwarte 5, Tautenburg, 07778 Tautenburg, Germany
e-mail: davide.gandolfi@esa.int
[2] Research and Scientific Support Department, ESTEC/ESA, PO Box 299, 2200 AG Noordwijk, The Netherlands
[3] Institut d'Astrophysique de Paris, UMR7095 CNRS, Université Pierre & Marie Curie, 98bis boulevard Arago, 75014 Paris, France
[4] Observatoire de l'Université de Genève, 51 chemin des Maillettes, 1290 Sauverny, Switzerland
[5] Laboratoire d'Astrophysique de Marseille, 38 rue Frédéric Joliot-Curie, 13388 Marseille Cedex 13, France
[6] McDonald Observatory, University of Texas at Austin, Austin, TX 78712, USA
[7] Institute of Planetary Research, German Aerospace Center, Rutherfordstrasse 2, 12489 Berlin, Germany
[8] Université de Nice-Sophia Antipolis, CNRS UMR 6202, Observatoire de la Côte d'Azur, BP 4229, 06304 Nice Cedex 4, France
[9] Oxford Astrophyiscs, Denys Wilkinson Building, Keble Road, Oxford OX1 3RH, UK
[10] LESIA, Observatoire de Paris, Place Jules Janssen, 92195 Meudon Cedex, France
[11] Institut d'Astrophysique Spatiale, Université Paris XI, 91405 Orsay, France
[12] Observatoire de Haute Provence, 04670 Saint Michel l'Observatoire, France
[13] LUTH, Observatoire de Paris, CNRS, Université Paris Diderot, 5 place Jules Janssen, 92195 Meudon, France
[14] Rheinisches Institut für Umweltforschung an der Universität zu Köln, Aachener Strasse 209, 50931 Köln, Germany
[15] Instituto de Astrofísica de Canarias, 38205 La Laguna, Tenerife, Spain
[16] University of Vienna, Institute of Astronomy, Türkenschanzstr. 17, 1180 Vienna, Austria
[17] IAG, University of São Paulo, Brasil
[18] University of Liège, Allée du 6 août 17, Sart Tilman, Liège 1, Belgium
[19] European Southern Observatory, Alonso de Crdova 3107, Casilla 19001, Santiago de Chile, Chile
[20] Space Research Institute, Austrian Academy of Science, Schmiedlstr. 6, 8042 Graz, Austria
[21] School of Physics and Astronomy, Raymond and Beverly Sackler Faculty of Exact Sciences, Tel Aviv University, Tel Aviv, Israel
[22] Center for Astronomy and Astrophysics, TU Berlin, Hardenbergstr. 36, 10623 Berlin, Germany
[23] Dpto. de Astrofísica, Universidad de La Laguna, 38206 La Laguna, Tenerife, Spain
[24] Laboratoire d'Astronomie de Lille, Université de Lille 1, 1 impasse de l'Observatoire, 59000 Lille, France
[25] Institut de Mécanique Céleste et de Calcul des Ephémérides, UMR 8028 du CNRS, 77 avenue Denfert-Rochereau, 75014 Paris, France